Dalton Transactions

Accepted Manuscript

ROYAL SOCIETY OF CHEMISTRY

www.rsc.org/dalton

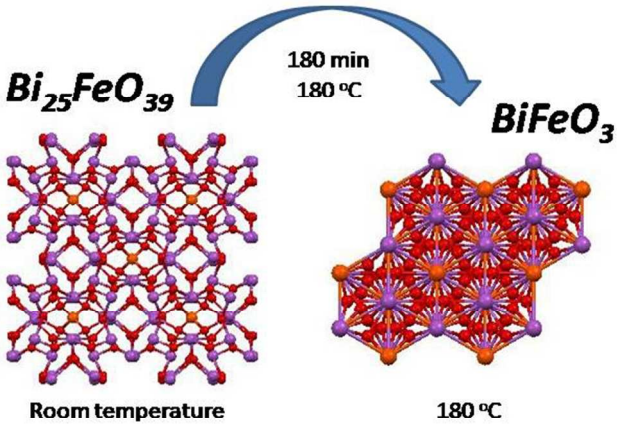

Sillentite-type Bi25FeO39 is synthesized at room temperature and its kinetic relations with rombohedrally distorted perovskite-type BiFeO3 are revealed.
254x190mm (96 x 96 DPI)

Room temperature synthesis of $Bi_{25}FeO_{39}$ and hydrothermal kinetic relations between sillenite- and distorted perovskite-type bismuth ferrites

Armandina M. L. Lopes [a, b], *João P. Araújo* [a], *Stanislav Ferdov* * [c]

[a] *IFIMUP and IN-Institute of Nanoscience and Nanotechnology, Department of Physics and Astronomy, Faculty of Sciences, University of Porto, 4169-007 Porto, Portugal.*

[b] *Centre for Nuclear Physics of the University of Lisbon, P-1649-003 Lisbon, Portugal*

[c] *Department of Physics, University of Minho, 4800-058 Guimarães, Portugal*

**Tel. +351 253 510 468; Fax + 351 253 510 461; E-mail address: sferdov@fisica.uminho.pt*

†Electronic supplementary information (ESI) available: Rietveld refinement plot of the phase quantification (Figure S1), atomic coordinates and isotropic parameters for the refined phases (Tables S1-S3). CSD numbers 428378, 428379 and 428380 contain complete crystallographic data for $Bi_{25}FeO_{39}$ (RT and HT) and $BiFeO_3$. Figures S2 and S3 show non linear reciprocal susceptibility versus temperature and isothermal magnetization versus magnetic field with corresponding fit for $Bi_{25}FeO_{39}$ samples.

Abstract

Time-dependent study at mild hydrothermal conditions revealed kinetic relation between structurally unrelated bismuth ferrites. We report synthesis conditions that disclose *in situ* transformation of $Bi_{25}FeO_{39}$ into $BiFeO_3$ only by extending the time for crystallization. We also demonstrate how careful investigation of the early stages of multiferroics crystallization provides cheap and easy room-temperature access to important sillenite-type of structure of $Bi_{25}FeO_{39}$. Crystal structure analysis by the method of Rietveld and

magnetization measurements provided detailed structure and magnetic relations between the synthesis conditions and the properties of the run product. The $BiFeO_3$ antiferromagnetic behavior with a small ferromagnetic component arising from particles surface uncompensated spins is ascertained.

Introduction

Bismuth compounds with sillenite- and rhombohedrally distorted perovskite-type of structure attract a great interest due their versatile properties.[1] Sillenites ($Bi_{12}MO_{20}$, M = Fe, V, Ge, Ti and etc.) are widely studied because of their photo-refractivity, optical activity, photo-conductivity, piezomodulus and an enhanced velocity of ultrasound wave propagation which make them a potential candidate for elaboration of electro-optic, acoustic and piezoelectric devices.[2-5] Perovskite-type members of the family ($BiFeO_3$ and $BiMnO_3$) attracted even greater attention as they show coexistence of ferroelectricity and magnetic order.[6-8] In this respect, $BiFeO_3$ is an exceptional multi-ferroic material at room temperature[4] which has potential applications in information storage, spintronics and sensors.[9,10] The synthesis of these materials is usually performed by solid-state reaction which frequently results in coexistence of phases as $BiFeO_3$, $Bi_2Fe_4O_9$ and $Bi_{25}FeO_{39}$. Other disadvantages of this method are related with the high reaction temperature, difficult control of the reaction conditions and the large grain size of the run product. More recently, mild hydrothermal syntheses have appeared as alternative for preparation of bismuth ferrites of different sizes and morphology.[4] The potential of this method lies on the easier control of the product purity, low reaction temperature, good dispersion, controllable grain size, and low production costs. A common practice in the hydrothermal synthesis of bismuth ferrites is the use of alkaline chemical sources (KOH and NaOH) as mineralizators[11, 12] and temperatures that usually range between 180 and 270 ^oC.[4] An exception from these values is a recent report on ethanol-assisted hydrothermal synthesis of $BiFeO_3$ achieved at 120 ^oC.[13] However, to the best our knowledge no room-temperature synthesis and time-dependent transformations between bismuth ferrites in hydrothermal conditions are reported.

In this study we report the first room temperature synthesis of $Bi_{25}FeO_{39}$ and reveal time-dependent transformation between sillenite- and rhombohedrally distorted perovskite-type of bismuth ferrites.

Experimental

Synthesis. Time-dependent transformation from $Bi_{25}FeO_{39}$ to $BiFeO_3$ were performed from a batch prepared by subsequent mixing of three solutions: (1) 1.21g of $Fe(NO_3)_3 \cdot 9H_2O$ (Sigma-Aldrich) dissolved in 6.0 g H_2O; (2) 1.46g $Bi(NO_3)_3 \cdot 5H_2O$ (Sigma-Aldrich) dissolved in 6 g of H_2O and 1.5 ml HNO_3 (70%) (Sigma-Aldrich) and (3) 42 g KOH (Sigma-Aldrich) dissolved in 6.0 g H_2O. The final mixture was homogenized by magnetic stirrer, placed in stainless steel Teflon-lined autoclave and heated at 180°C for 45, 90, 180 and 360 min. The room temperature synthesis was carried out from suspension prepared by mixing the following solutions: (1) 0.97 g $Bi(NO_3)_3 \cdot 5H_2O$ dissolved in 4.0 g H_2O and 1 ml HNO_3 (70%); (2) 0.81 g $Fe(NO_3)_3 \cdot 9H_2O$ dissolved in 4.0 g H_2O; (3) 27.8 g KOH dissolved 30 g H_2O. The obtained batch was homogenized by magnetic stirrer for 60 min at 80 °C and then left at room temperature (20-25 °C) for 20 h. The run products of all samples were filtered, washed with distilled water and dried at room temperature.

Characterization. The samples were analyzed by powder X-rays diffraction (XRD) using a Bruker D8 Discover diffractometer (CuKα radiation - λ=1.5406 Å, step 0.04°, time per step 20 s, 10-90° ($Bi_{25}FeO_{39}$) and 20-130° ($BiFeO_3$) 2θ interval. The amount of amorphous fraction was estimated by subtraction of the integrated area of the diffraction reflections from the total area of the XRD pattern. This was performed by the TOPAS software which allows full pattern decomposition and simultaneous fit of the amorphous and the crystalline fractions. The scanning electron microscopy images (SEM) and Energy Dispersive Spectroscopy (EDS) data were collected at the "Centro de Materiais da Universidade do Porto" with FEI Quanta 400FEG ESEM/EDAX Genesis X4M apparatus. Before the measurements the samples pellet surface was gently polished and mounted into the sample holder with carbon tape. The temperature dependent magnetic susceptibility χ (=M/H) measurements, performed between 4.5 and 320 K under a

H=50 Oe magnetic field, were acquired on samples using a commercial (Quantum Design) superconducting quantum interference device (SQUID) magnetometer. The measurements were performed using the zero field cooling (ZFC) and field cooling (FC) procedures. Isothermal magnetization at 4.5 and RT were acquired while sweeping the magnetic field from -5.5 up to 5.5 T.

Results and discussion

Fig. 1a shows the XRD pattern of $Bi_{25}FeO_{39}$ prepared at room temperature. The diffractogram is composed of diffraction peaks and amorphous bump centered around 30 2θ. More than 60% of the amorphous bismuth ferrite fraction is transformed into sillenite-type structure. Prolongation of the time for reaction (up to 168 h at room temperature) resulted in no change in the ratio between the crystalline and amorphous phase, which suggests the need for higher temperature of synthesis. As shown in Fig. 1b-d, at 180 ^{o}C and hydrothermal conditions $Bi_{25}FeO_{39}$ is readily synthesized in a very short time. Extending the time for crystallization revealed a kinetic relation between the sillenite and distorted perovskite-type of bismuth ferrites. This shows that at certain conditions $Bi_{25}FeO_{39}$ is metastable phase and gradually transforms into more stable $BiFeO_3$.Thus, after 45 min of synthesis a $Bi_{25}FeO_{39}$ is formed. Increasing the time up to 180 min the sillenite phase transforms into rhombohedrally distorted perovskite-type $BiFeO_3$ which remains unchanged when the time for crystallization is extended up to 120 h. In intermediate time of 90 min (Fig. 1c) a mixture between $Bi_{25}FeO_{39}$ (93 %) and $BiFeO_3$ (7%) is observed (Fig. S1).

SEM images of the as-synthesized phases are shown in Figs. 3 and 4. $Bi_{25}FeO_{39}$ obtained at room temperature is in form of isolated particles incorporated in shapeless lumps of amorphous phase (Fig. 3 a,b). Increasing the temperature up to 180 ^{o}C and synthesis time to 45 min and subsequently to 90 min led to greater number of well-defined particles of $Bi_{25}FeO_{39}$ (Fig. 3 c-f). Although there is no clear evidence for X-ray amorphous phase, similar shapeless mass as in the room temperature run product is also present. This suggests the existence of discrete crystalline product or relatively low amount of amorphous phase. Probing the chemical composition indicated that the concentration of iron in the shapeless mass (Fe:Bi = 4) is much higher than in the particles of $Bi_{25}FeO_{39}$. This is logical, considering that the ratio Bi:Fe in the

initial batch is 1:1 and in $Bi_{25}FeO_{39}$ is 25:1, and then in the final product of $BiFeO_3$ the ratio returns to 1:1. Fig. 4 shows ball-like agglomerates of $BiFeO_3$ prepared at 180 ^oC for 180 and 360 min. The SEM images demonstrate that up to 180 min of synthesis time the lumps of shapeless mass are decorated with well-shaped particles that later transform into bigger crystals at the expense of the shapeless mass.

The structures and phase purity of all synthesized phases were confirmed by the method of Rietveld using TOPAS-3 software package (Bruker AXS, Karlsruhe, Germany). Details from the Rietveld refinement are reported in Table 1. Refined atomic coordinates and isotropic and displacement parameters are shown in Tables S1-S3. Selected inter-atomic distances of the refinement are gathered in Tables 2-4. The observed, calculated, and difference profiles are given in Fig. 2a-c.

The powder XRD patterns of $Bi_{25}FeO_{39}$ (room temperature and hydrothermal synthesis) were indexed using the cubic sillenite-type structure in the body-centered *I*23 space group. The crystal structure was refined starting from previously reported structural model of $Bi_{25}FeO_{39}$.[14] Within the experimental error the Rietveld refinement showed that there is no difference between the room temperature and hydrothermally prepared $Bi_{25}FeO_{39}$.The lattice dimensions of the hydrothermally prepared sample are only about 0.04% larger than the one obtained at room temperature (Table 1).

In both samples the tetrahedral site (2a) was refined as equally shared bismuth (Bi^{3+}) and iron (Fe^{3+}) ions. The obtained tetrahedral environment is regular with Bi/Fe-O distances that vary between 1.8816(7) Å (RT synthesis) and 2.1689(2) Å (hydrothermal synthesis). This bond length difference may due to disorder between the Bi^{3+} and Fe^{3+} ions occupying the same site. The coordination polyhedron of the Bi atom occupying the 24(f) site corresponds to a distorted octahedron with Bi-O distances ranging from 1.8999(9) to 2.5848(7) Å (RT synthesis), and from 2.0607(1) to 2.4917(1) Å (HT hydrothermal synthesis).The obtained bond distances are in a fair agreement with the previously reported ones in the starting model.

Fig. 2c shows the Rietveld plot of $BiFeO_3$. The powder XRD pattern was indexed using the distorted rhombohedral structure with *R*3c space group. The staring model for the refinement was the previously reported single crystal data for $BiFeO_3$.[15] The Fe atoms are coordinated by six O atoms

forming a distorted octahedron with three short (1.8960(1) Å) and three long (2.1689(2) Å) bonds. In a similar way the Bi atom is octahedrally coordinated with three short (2.3332(1) Å) and three long (2.4901(2) Å) bonds (Table 3) which is in accordance with the previously reported structural data.[15] The refined structural results confirmed the successful synthesis of phase pure $BiFeO_3$ at mild hydrothermal conditions.

The magnetization (FC and ZFC) as a function of temperature measured at low applied field (H=50 Oe) is presented in Fig. 5. For all the samples the susceptibility shows a monotonic increase upon cooling and a bifurcation between the ZFC and the FC curves below 56 K. The presented magnetization behavior is similar to the reported in literature for the $Bi_{25}FeO_{39}$ and nano-sized $BiFeO_3$,[16-18] in particular for $Bi_{25}FeO_{39}$ prepared by hydrothermal syntheses method.[18] The broad maximum in the ZFC curve (Tmax) and the ZFC–FC bifurcation has been attributed to spin-glass-like freezing occurring in $BiFeO_3$[17-19] as well as in $Bi_{25}FeO_{39}$.[16] Increasing the crystallization of $Bi_{25}FeO_{39}$, by a 45 min of thermal treatment at 180 ^oC, an increase of the magnetization values and Tmax is observed.

The hysteresis loops at 4.5 K and at room temperature for $Bi_{25}FeO_{39}$ prepared at room temperature and after 45 min at 180 ^oC are shown in Fig. 6. For the sample prepared at RT a sharp increase of the magnetization at low fields and a clear tendency for saturation at fields around 5 Tesla is apparent at 4.5 K. Additionally a coercive field of 430 Oe and a Mr/Ms=0.15 coefficient is obtained (Ms, saturation magnetization, stands for the saturation magnetization at 5.5 tesla and Mr for remanent magnetization). The hysteresis loops measured at room temperature show no noticeable coercive field or remanent magnetization. Upon thermal treatment an increase of the magnetization values and a decrease of the coercive field to 180 Oe and Mr/Ms=0.06 is observed. Also here, at room temperature, no noticeable hysteresis is observed.

Although the above described magnetic behavior is well consistent with the literature,[18,20] one should mention that the magnetization values measured in both $Bi_{25}FeO_{39}$ samples are well above of those expected for a pure phase ($Ms=5\mu_B$ per Fe^{3+}). This suggests that the process of phase transformation pass

though hidden states of discrete crystalline and/or amorphous magnetic phases that have a substantial contribution to the magnetization data.

In fact, in the literature, the $Bi_{25}FeO_{39}$ magnetic behavior is attributed either to superparamagnetism, paramagnetism or ferromagnetism. Also a high dispersion on the magnetization values has been reported.[18, 20, 26-29] Yet, the most recent literature quotes $Bi_{25}FeO_{39}$ as a paramagnetic material down to the lowest temperatures[28, 29]. In this case $Bi_{25}FeO_{39}$ follows the Curie-Weiss law, i.e, $\chi = \frac{C}{T-\theta_p}$, with $\theta_p \sim 0$ (C and θ_p are the Curie-Weiss constant and temperature, respectively). The experimental effective magnetic moments (μ_{eff} in terms of the Bohr magneton unit, μ_B) can thus be obtained from: $C = N \mu^2_{eff}/3k_B$, where N is the Avogadro number and k_B is the Boltzmann constant, which can be compared with the theoretical value $\mu=5.92\ \mu_B$ for the Fe^{3+} high-spin state, neglecting spin orbital interactions. However, in our work the χ^{-1} expected linearity is not observed (see Fig S2) and the Curie-Weiss law cannot be applied.

Additionally, and as referred above, our low temperature isothermal M(H) curves are not consistent with the theoretical saturation magnetic moment of a Fe^{3+} high-spin state (S=5/2), μ_{sat} =5.0 μ_B, expected for a $Bi_{25}FeO_{39}$ single phase. In fact, based in our x-ray and magnetization results and in the most recent literature the $Bi_{25}FeO_{39}$ samples prepared at room temperature and 180 ºC present a superposition of paramagnetic (PM) behavior arising from the $Bi_{25}FeO_{39}$ phase and superparamagnetism (SPM) arising from iron oxide e.g. γ- Fe_2O_3, α-Fe_2O_3 or Fe_3O_4 amorphous or nanocrystalline phases [30-33]. Indeed our room temperature M(H) curves are well fitted by a Langevin function, accounting for SPM, with an added linear term, accounting for PM, thus demonstrating the superposition of these two magnetic contributions (see Fig S3).

Magnetization data as a function of the temperature of $BiFeO_3$ show a clear decrease of the magnetization values and a Tmax around 56K (see Fig. 5 bottom) consistent with the results presented in the literature for subcrystalline samples.[16-18] The isothermal curves depicted in Fig. 7, as expected, evidence the presence of antiferromagnetism with a small ferromagnetic component. At low temperatures, 4.5 K, a magnetization value of Ms=1.85 emu/g at 5.5 tesla, a coercive field of 300 Oe and Mr=0.1 emu/g

(Mr/Ms=0.05) is obtained. The measurements at RT show a magnetization decreasing (M=1.4 emu/g at 5.5 tesla) and no significant coercive field and remnant magnetization is observed. The magnetization values obtained here are much lower than the ones obtained by combustion reaction, employing tartaric acid.[21] In fact they are quite similar to the ones obtained in the same reference using glycine as ligand where it is claimed that no undesirable secondary magnetic phases are present in their system. In a similar manner the high M~2.9 emu/g value obtained for $BiFeO_3$ prepared by hydrothermal synthesis in reference[16] is attributed to unpaired spins in the amorphous/sub-crystalline $BiFeO_3$ interface.

Although, Fe_3O_4[22] or $Bi_{25}FeO_{39}$[23] magnetic impurities are ascribed as responsible for the huge magnetic moment observed in nanocrystalline multiferroic $BiFeO_3$ our analyses showed no X-ray reflections of secondary phase. Thus, the weak ferromagnetism could due to discrete amount of unconverted metastable phasethat is under the resolution limits (~1 %) of X-ray diffraction, or to BiFeO3 nano/micro-particles, whose enhanced ferromagnetism can be attributed to the breaking of the spin cycloid structure periodicity, characteristic of bulk $BiFeO_3$.[17,18,24]

When the time for crystallization is increased up to 360 min a clear change in the magnetic behavior of $BiFeO_3$ is observed (Fig. 8). It is apparent a linear increase of the magnetization with the rise of the magnetic field which is typical for an antiferromagnetic system. A coercive field of 850 Oe and a 0.03 emu/g remnant magnetization is measured at 4.5 K. The magnetization at 5.5 tesla, 0.50 emu/g, decreases to 0.45 emu/g at room temperature. At this temperature no remnant magnetization is observed.

According to the results of Huang et al.[17] and Park et al.,[18] a ferromagnetic component observed in antiferromagnetic ordered $BiFeO_3$ can be explained by particle size effects since long-range antiferromagnetic order, is interrupted at the nanoparticle surfaces and the uncompensated ferromagneticaly ordered spins will contribute to the net magnetization. As the surface-volume ratio decreases, with increasing particle size, the ferromagnetic contributions will decrease. In this context, a decrease of the saturation magnetization and coercive field increase can be explained in terms of the larger size of the $BiFeO_3$ crystals. Additionally, a similar argument, missing structural order in grain boundaries that generates uncompensated spins, is used to explain the enhanced magnetization (M~0.5

emu/g at 5 tesla, 5K) in particles with average grain size around 1.2 μm.[24] Intrinsic weak ferromagnetism has also been observed in $BiFeO_3$ thin films under strain, where the magnetic cycloid is suppressed.[25] Accordingly our structural and magnetic results, in $BiFeO_3$, agree well with the existence of FM component within the antiferromagnetic order arising from the grain boundaries, where the spin helix structure order is broken.

Conclusions

In this study, time-dependent transformation of $Bi_{25}FeO_{39}$ into $BiFeO_3$ is revealed. Kinetic studies in hydrothermal conditions showed the metastable character of the sillenite-type structure, which bring a new insight in the mechanism of crystallization of bismuth ferrites. Exploring the metastable behavior of $Bi_{25}FeO_{39}$ we demonstrated the first room temperature synthesis of sillenite-type bismuth ferrite. From an economical perspective, the synthesis of $Bi_{25}FeO_{39}$ presented here is attractive, as crystalline solid can be easily synthesized at ambient temperature and atmospheric pressure without using autoclaves, suggesting that scale-up of an energy-efficient synthesis would be feasible. Finally, the obtained phases were characterized in detail by X-ray diffraction and magnetization analyses. In particular for the $BiFeO_3$ sample an antiferromagnetic behavior with a small ferromagnetic component, coherent with the breaking of the spin cycloid structure periodicity in the particles surface is observed.

Acknowledgements

This work was supported by the Fundaçãopara a Ciência e a Tecnologia (FCT) – "Investigador 2013", and projects NORTE-07-0124- FEDER-000070, PTDC/FIS-NAN/0533/2012, PTDC/CTM-NAN/115125/2009 and CERN/FP/123585/2011.

References

1. M. Valant and D. Suvorov, *Chemistry of Materials*, 2002, **14**, 3471-3476.

2. E. Nippolainen, A. A. Kamshilin, V. V. Prokofiev and T. Jaaskelainen, *Applied Physics Letters*, 2001, **78**, 859-861.

3. H. J. Reyher, U. Hellwig and O. Thiemann, *Physical Review B*, 1993, **47**, 5638-5645.

4. J.-T. Han, Y.-H. Huang, X.-J. Wu, C.-L. Wu, W. Wei, B. Peng, W. Huang and J. B. Goodenough, *Advanced Materials*, 2006, **18**, 2145-2148.

5. M. Zaleski, *Journal of Applied Physics*, 2000, **87**, 4279-4284.

6. N. Hur, S. Park, P. A. Sharma, J. S. Ahn, S. Guha and S. W. Cheong, *Nature*, 2004, **429**, 392-395.

7. J. Wang, J. B. Neaton, H. Zheng, V. Nagarajan, S. B. Ogale, B. Liu, D. Viehland, V. Vaithyanathan, D. G. Schlom, U. V. Waghmare, N. A. Spaldin, K. M. Rabe, M. Wuttig and R. Ramesh, *Science*, 2003, **299**, 1719-1722.

8. E. Montanari, L. Righi, G. Calestani, A. Migliori, E. Gilioli and F. Bolzoni, *Chemistry of Materials*, 2005, **17**, 1765-1773.

9. T. J. Park, G. C. Papaefthymiou, A. R. Moodenbaugh, Y. B. Mao and S. S. Wong, *Journal of Materials Chemistry*, 2005, **15**, 2099-2105.

10. W. Eerenstein, N. D. Mathur and J. F. Scott, *Nature*, 2006, **442**, 759-765.

11. C. Chen, J. R. Cheng, S. W. Yu, L. J. Che and Z. Y. Meng, *Journal of Crystal Growth*, 2006, **291**, 135-139.

12. H. Jiang, Y. Morozumi, N. Kumada, Y. Yonesaki, T. Takei and N. Kinomura, *Journal of the Ceramic Society of Japan*, 2008, **116**, 837-839.

13. Z. Chen, Y. Wu and J. Hu, *Journal of the American Ceramic Society*, **96**, 1345-1348.

14. D. C. Craig and N. C. Stephenson, *Journal of Solid State Chemistry*, 1975, **15**, 1-8.

15. F. Kubel and H. Schmid, *Acta Crystallographica Section B-Structural Science*, 1990, **46**, 698-702.

16. F. Z. Huang, Z. J. Wang, X. M. Lu, J. T. Zhang, K. L. Min, W. W. Lin, R. X. Ti, T. T. Xu, J. He, C. Yue and J. S. Zhu, *Scientific Reports*, 2013, **3**, 1-7.

17. T. J. Park, G. C. Papaefthymiou, A. J. Viescas, A. R. Moodenbaugh and S. S. Wong, *Nano Letters*, 2007, **7**, 766-772.

18. L. Wu, C. H. Dong, H. Chen, J. L. Yao, C. J. Jiang and D. S. Xue, *Journal of the American Ceramic Society*, 2012, **95**, 3922-3927.

19. M. K. Singh, W. Prellier, M. P. Singh, R. S. Katiyar and J. F. Scott, *Physical Review B*, 2008, **77**.

20. G. Q. Tan, Y. Q. Zheng, H. Y. Miao, A. Xia and H. J. Ren, *Journal of the American Ceramic Society*, 2012, **95**, 280-289.

21. J. L. Ortiz-Quinonez, D. Diaz, I. Zumeta-Dube, H. Arriola-Santamaria, I. Betancourt, P. Santiago-Jacinto and N. Nava-Etzana, *Inorganic Chemistry*, 2013, **52**, 10306-10317.

22. S. Vijayanand, H. S. Potdar and P. A. Joy, *Applied Physics Letters*, 2009, **94**, 182507-3

23. L. C. Wang, Z. H. Wang, S. L. He, X. Li, P. T. Lin, J. R. Sun and B. G. Shen, *Physica B-Condensed Matter*, 2012, **407**, 1196-1202.

24. D. Lebeugle, D. Colson, A. Forget, M. Viret, P. Bonville, J. F. Marucco and S. Fusil, *Physical Review B*, 2007, **76**, 024116-8.

25. M. Ramazanoglu, M. Laver, W. Ratcliff, S. M. Watson, W. C. Chen, A. Jackson, K. Kothapalli, S. Lee, S. W. Cheong and V. Kiryukhin, *Physical Review Letters*, 2011, **107**, 207206-5.

26 Y. Sun, X. Xiong, Z. Xia, H. Liu, Y. Zhou, M. Luo, C. Wang, Ceramics International, 2013, **39**, 4651–4656.

27 A. Sun, H. Chen, C. Song, F. Jiang, X. Wang, Environmental Chemistry, 2013, **32** 748–754.

28 A.A. Zatsiupa, L.A. Bashkirov, I.O. Troyanchuk, G.S. Petrov, A.I. Galyas, L.S. Lobanovsky, S.V. Truhanov, Journal of Solid State Chemistry, 2014, **212**, 147–150.

29 R. Koferstein, T. Buttlar, S.G. Ebbinghaus, Journal of Solid State Chemistry, 2014, accepted manuscript http://dx.doi.org/ 10.1016/j.jssc.2014.05.006.

30 T. Sharifi, E. Gracia-Espino, H. R. Barzegar, X. Jia, F. Nitze, G. Hu, P. Nordblad, C-W Tai, and T. Wagberg, Nature Communications, 2013, 4, 2319-9.

31 J. S. Salazar, L. Perez, O. de Abril, L. T. Phuoc, D. Ihiawakrim, M. Vazquez, J-M Greneche,S. Begin-Colin, and G Pourroy, Chemistry of Materials, 2011, **23**, 1379–1386.

32 H. Khurshid, W. Li, M-H Phan, P Mukherjee, G.C. Hadjipanayis, and H. Srikanth, Applied Physics Letters, 2012, **101**, 022403-5.

33 W. Wu, X.H. Xiao, S.F. Zhang, T.C. Peng J. Zhou, F.Ren, C.Z. Jiang, Nanoscale Research Letters, 2010, **5**, 1474–1479.

Table 1. Crystallographic data for the refined compounds.

Sample	$Bi_{25}FeO_{39}$	$Bi_{25}FeO_{39}$*	$BiFeO_3$
Formula weight (g/mol)	5920.3(3)	5920.3(3)	312.8(2)
Range in 2θ, step size (^{o})	10-90, 0.04	10-90, 0.04	20-130, 0.04
Crystal system	cubic	cubic	trigonal
Spacegroup	*I*23	*I*23	*R*3cH
Unit cell parameters			
a (Å)	10.1750(1)	10.1736(1)	5.58350(2)
c(Å)			13.87354(5)
Volume (Å^3)	1053.42(8)	1052.99(1)	374.568(3)
Rp %	4.23	3.48	5.31
Rwp %	5.34	4.32	6.99
R_B %	2.62	0.84	1.66
Goodness of fit	1.49	1.13	1.62

* prepared at room temperature (20-25 ^{o}C)

Table 2. Selected bond distances for the refined $Bi_{25}FeO_{39}$*.

Atom1	Atom2	Count	d 1,2 (Å)
Bi1	O2	1x	2.0607(1)
	O1	1x	2.2044(4)
	O2	1x	2.2714(5)
	O3	1x	2.4917(1)
Bi2|Fe	O3	4x	2.1376(9)

Table 3. Selected bond distances for the refined $Bi_{25}FeO_{39}$.

Atom1	Atom2	Count	d 1,2 (Å)
Bi1	O2	1x	1.8999(9)
	O1	1x	2.1941(3)
	O2	1x	2.2999(6)
	O3	1x	2.5848(7)
Bi2|Fe	O3	4x	1.8816(7)

Table 3. Selected bond distances for the refined $BiFeO_3$.

Atom1	Atom2	Count	d 1,2 (Å)
Bi1	O1	3x	2.3332(1)
	O1	3x	2.4901(2)
Fe	O1	3x	1.8960(1)
	O1	3x	2.1689(2)

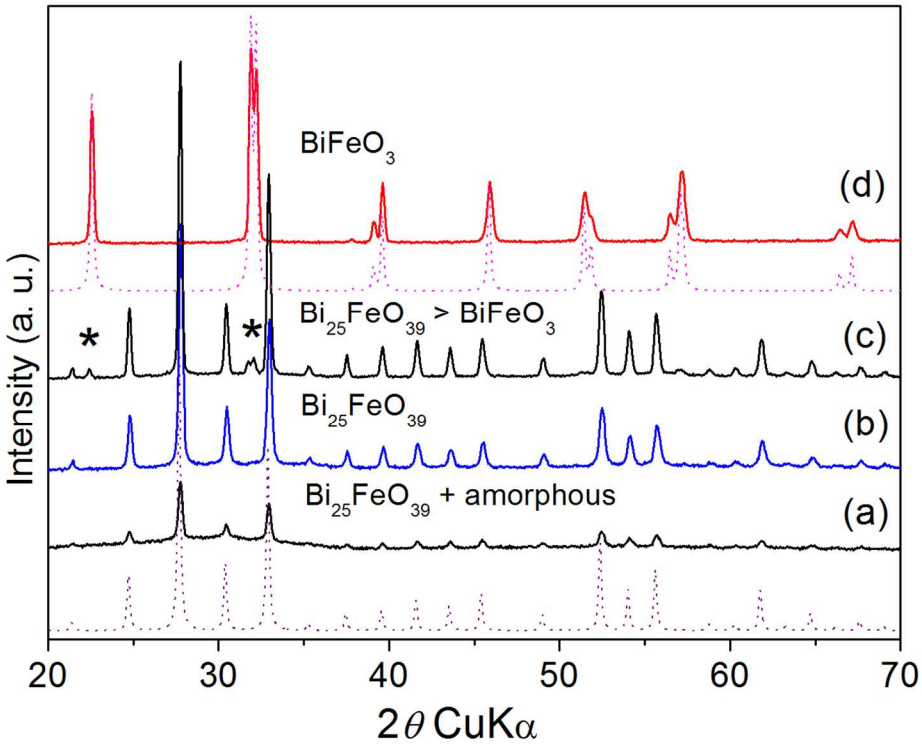

Fig. 1. Powder XRD patterns of bismuth ferrites prepared at room temperature (a) and at 180 ^{o}C for 45 min (b), 90 min (c) and 180 min (d). The asterisks indicate impurity of $Bi_{25}FeO_{39}$. Dotted curves are the calculated powder XRD patterns of the related phases.

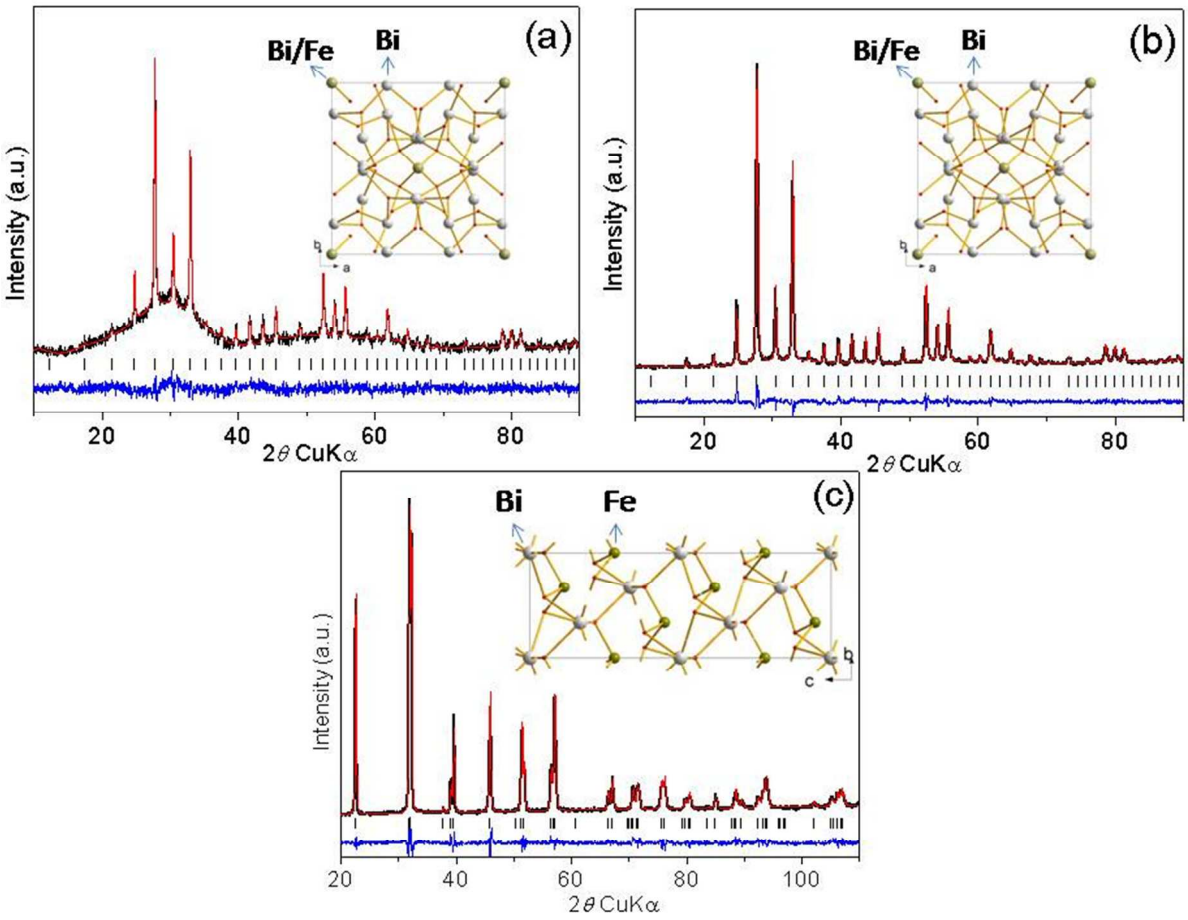

Fig. 2. Rietveld refinement plots of $Bi_{25}FeO_{39}$ prepared at room temperature (a); $Bi_{25}FeO_{39}$ prepared at 180 ^{o}C for 90 min (b) and $BiFeO_3$ prepared for 360 min. Black curve (experimental), red curve (calculated). The insets show the related crystal structure generated from the refined data.

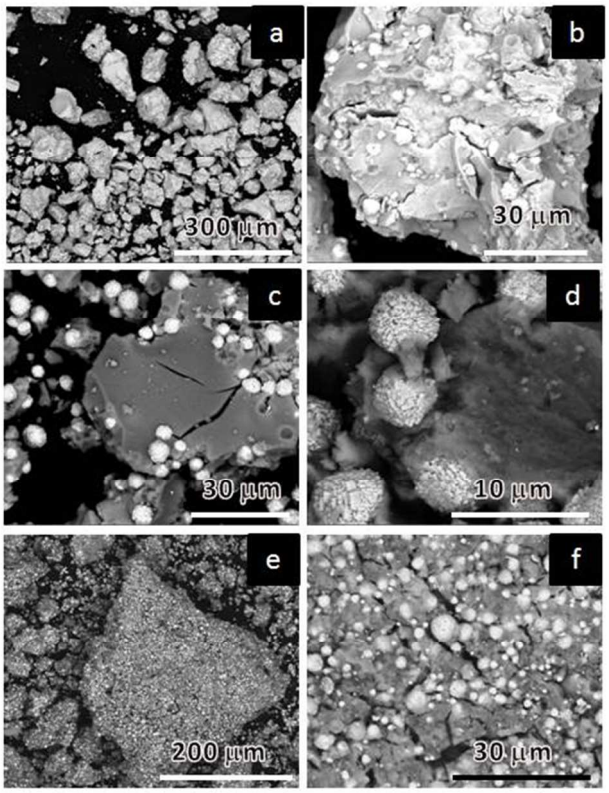

Fig. 3. SEM images of $Bi_{25}FeO_{39}$ prepared at room temperature (a, b); $Bi_{25}FeO_{39}$ prepared at 180 ^{o}C for 45 min (c, d) and 90 min (e, f).

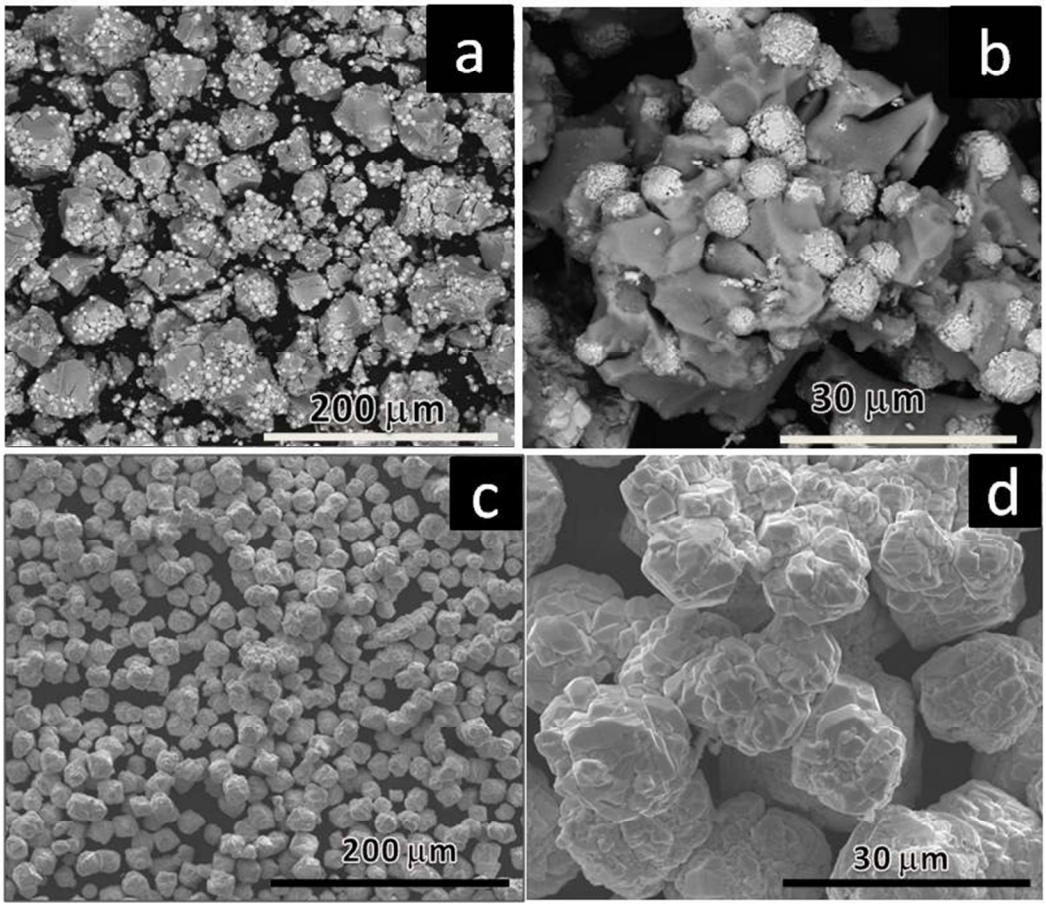

Fig. 4. SEM images of $BiFeO_3$ prepared at 180 ^{o}C for 180 min (a, b) and 360 min (c, d).

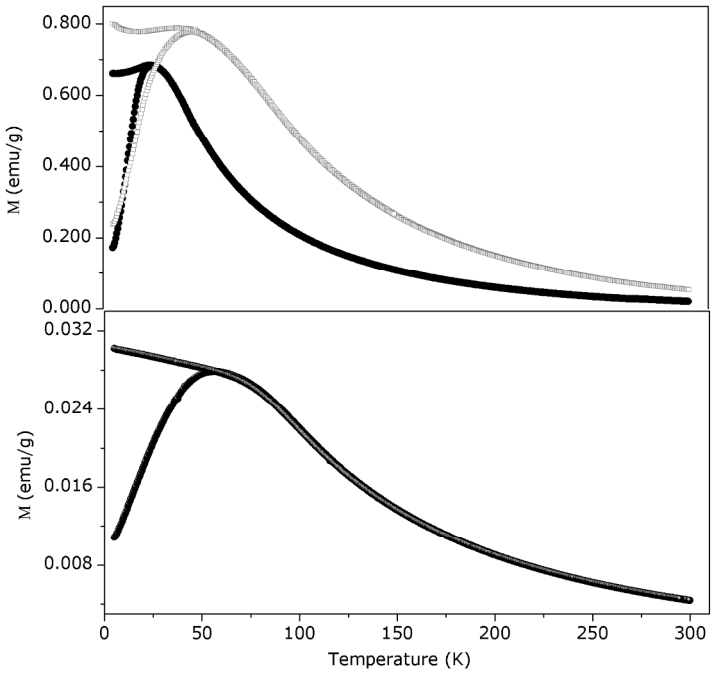

Fig. 5. Temperature dependence of the field-cooled (FC) and zero field-cooled (ZFC) magnetization for $Bi_{25}FeO_{39}$ prepared at room temperature (top black curve), $Bi_{25}FeO_{39}$ prepared at 180 ^{o}C for 45 min (top gray curve) and $BiFeO_3$ (bottom) measured in a H=50 Oe applied magnetic field.

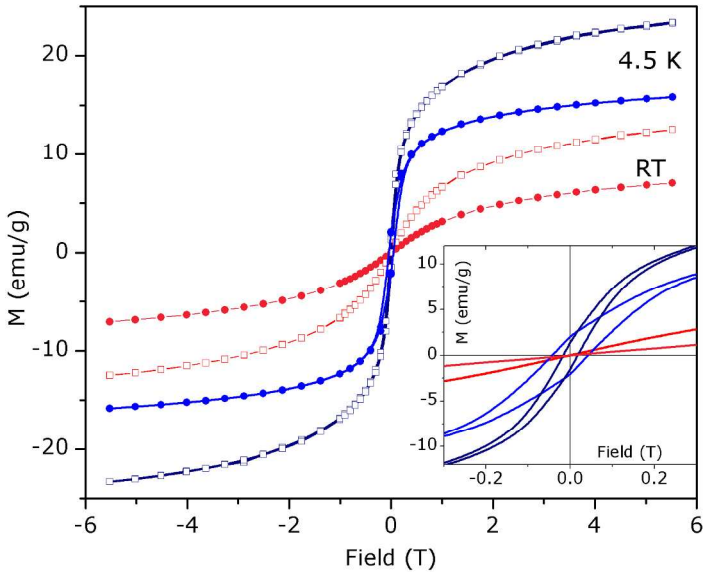

Fig. 6. Magnetic hysteresis loops for $Bi_{25}FeO_{39}$ prepared at room temperature (dots) and prepared at 180 ^{o}C for 45 min (open squares), measured at 4.5 K (blue) and room temperature (red). The inset shows the scaling-up images.

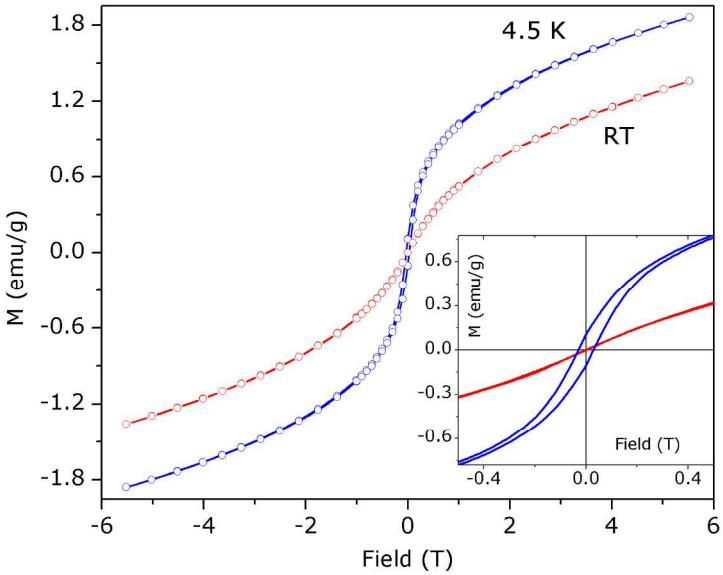

Fig. 7. Magnetic hysteresis loops for $BiFeO_3$prepared at 180 ^oC for 180 min measured at 4.5 K (blue) and at room temperature (red). The inset shows the scaling-up images.

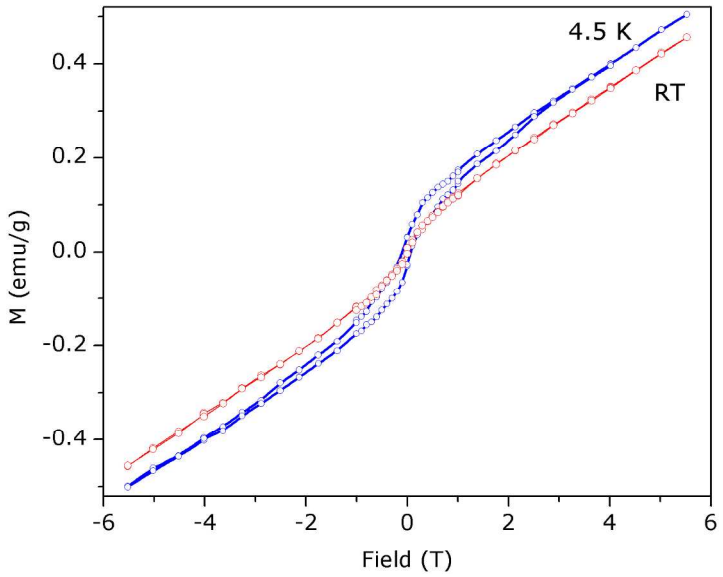

Fig. 8. Magnetic hysteresis loops for $BiFeO_3$ prepared at 180 ^oC for 360 min measured at 4.5 K (blue) and at room temperature (red).